CHAPTER TWO

Deregulation of the ubiquitin-proteasome system is the predominant molecular pathology in OPMD animal models and patients

Seyed Yahya Anvar[1], Peter A.C. 't Hoen[1], Andrea Venema[1], Barbara van der Sluijs[2], Baziel van Engelen[2], Marc Snoeck[3], John Vissing[4], Capucine Trollet[5,6], George Dickson[5], Aymeric Chartier[7], Martine Simonelig[7], Gert-Jan B van Ommen[1], Silvère M. van der Maarel[5] and Vered Raz[1,*]

Oculopharyngeal muscular dystrophy (OPMD) is a late-onset progressive muscle disorder caused by a poly-alanine expansion mutation in PABPN1. The molecular mechanisms that regulate disease onset and progression are largely unknown. In order to identify molecular pathways that are consistently associated with OPMD, we performed an integrated high-throughput transcriptome study in affected muscles of OPMD animal models and patients. The ubiquitin-proteasome system (UPS) was found as the most consistently and significantly deregulated pathway across species. We could correlate the association of the UPS deregulated genes with stages of disease progression. The expression trend of a subset of these genes is age-associated and therefore marks the late onset of the disease, and a second group with expression trends relating to disease-progression. We demonstrate a correlation between expression trends and entrapment in PABPN1 insoluble aggregates of deregulated E3 ligases. We also show that manipulations of proteasome and immunoproteasome activity specifically affect the accumulation and aggregation of mutant PABPN1. We suggest that the natural decrease in proteasome expression and its activity during muscle aging contributes to the onset of the disease.

1 Center for Human and Clinical Genetics, Leiden University Medical Center, Leiden, the Netherlands. **2** Department of Neurology, Radboud University Nijmegen Medical Centre, Nijmegen, the Netherlands. **3** Department of Anaesthesia, Canisius-Wilhelmina Hospital, Nijmegen, the Netherlands. **4** Neuromuscular Research Unit and Department of Neurology, University of Copenhagen, Rigs Hospitalet, Denmark. **5** School of Biological Sciences, Royal Holloway, University of London, Egham, UK. **6** INSERM U974, UMR 7215 CNRS, Institut de Myologie, UM 76 Université Pierre et Marie Curie, Paris, France. **7** Institut de Genetique Humaine, CNRS UPR1142, 141 rue de la Cardonille, 34396 Montpellier Cedex 5, France.

* To whom correspondence should be addressed at: v.raz@lumc.nl

Skeletal Muscle, 2011, Apr 4;1(1):15; doi:10.1186/2044-5040-1-15

BACKGROUND

Oculopharyngeal muscular dystrophy (OPMD) is a late-onset progressive muscle disorder for which the underlying molecular mechanisms are largely unknown. This autosomal dominant muscular dystrophy has an estimated prevalence of 1 in 100,000 worldwide (Fan and Rouleau, 2003). A higher prevalence has been reported in the Jewish Caucasian and French-Canadian populations (1 in 600 and 1 in 1000, respectively) (Blumen et al., 2009; Brais et al., 1995). OPMD is caused by expansion of a homopolymeric alanine (Ala) stretch at the N-terminus of the Poly(A) Binding Protein Nuclear 1 (PABPN1) by 2-7 additional Ala residues (Brais et al., 1998). Although PABPN1 is ubiquitously expressed, the clinical and pathological features of OPMD are restricted to a subset of skeletal muscles, causing progressive *ptosis*, *dysphagia*, and limb muscle weakness. In affected muscles, the expanded PABPN1 (expPABPN1) accumulates in intranuclear inclusions (INI) (Tome and Fardeau, 1980). Animal models for OPMD were generated in *Drosophila,* mouse and *C. elegans* with a muscle-specific expression of expPABPN1 (Chartier et al., 2006; Davies et al., 2005; Catoire et al., 2008). These models recapitulate INI formation and progressive muscle weakness in OPMD, and a correlation between INI formation and muscle weakness has been reported (Chartier et al., 2006; Davies et al., 2005; Catoire et al., 2008). In these OPMD models protein disaggregation approaches attenuate muscle symptoms (Davies et al., 2006; Catoire et al., 2008; Chartier et al., 2009). So far, however, the molecular mechanisms that are associated with OPMD onset and progression are not known. Previously, we preformed transcriptome analysis on skeletal muscles from a mouse model of OPMD and found massive gene deregulation, which was reflected by a broad spectrum of altered cellular pathways (Trollet et al., 2010). We found an association of transcriptional changes with muscle atrophy (Trollet et al., 2010). Muscle atrophy was recently reported in homozygous OPMD patients (Blumen et al., 2009). However, the vast majority of OPMD patients are heterozygous and muscle atrophy is not common pathological characteristic of the disease in its early stages. Importantly, a mouse model with low and constitutive expPABPN1 expression exhibits minor muscle defects without muscle atrophy (Hino et al., 2004). Hino et al. (2004) suggested that the extent of muscle symptoms caused by expPABPN1 depends on the expression level. Therefore, it is not known whether the massive transcriptional changes in affected muscles of the A17.1 OPMD model (Trollet et al., 2010) are due to the high over-expression of expPABPN1 or that they are common with transcriptional changes in OPMD patients.

We have generated microarrays of OPMD carriers at pre-symptomatic and symptomatic stages. Since OPMD is categorized as a rare disorder in Western countries, limited patient material is an obstacle in reaching conclusive results. Therefore, we performed a cross-species transcriptome study by integrating transcriptome data from *Drosophila* and mouse models and heterozygous OPMD patients. We hypothesized that OPMD-associated molecular mechanisms would be consistently deregulated across species. As bioinformatics analyses of gene expression are biased by the computational approaches (Ioannidis et al., 2009), here we integrated three computational methods to obtain a higher degree of confidence and reproducibility. The ubiquitin-proteasome system (UPS) was identified as the most significant and consistent OPMD-deregulated pathway across species.

RESULTS

Genome-wide expression profiles from the *Drosophila* and mouse OPMD models (Chartier et al., 2006; Trollet et al., 2010) were integrated with the expression profiles of heterozygous OPMD carriers (datasets are described in **Table S1** and **Table S2**). Genes that are differentially expressed between OPMD and controls (OPMD-deregulated) were identified using limma model in R

Table 1 - Deregulation of ubiquitin-proteasome system (UPS) in OPMD in *Drosophila,* human and mouse. For *Drosophila* and mouse *P*-values are derived from the combined analysis of the three time points using global test, where age was included as a confounder in the model.

	Drosophila	Mouse	Human
Literature Analysis			
Ubiquitination	# 2	# 1	# 1
GO Categories			
Ubiquitin-dependent Protein Catabolic Process	2.81E-04	2.27E-07	1.22E-03
Protein Ubiquitination	7.57E-03	1.88E-05	9.24E-04
Proteasomal Protein Catabolic Process	6.51E-03	2.23E-07	1.86E-03
KEGG Pathways			
Ubiquitin Mediated Proteolysis	2.03E-03	8.25E-08	1.52E-03
Proteasome	2.15E-04	1.37E-07	9.27E-03

(Smyth, 2004). To identify the most prominent and consistent feature across all species, comparative pathway analysis was performed using three computational methods (**Figure S1**). In literature-aided analyses (Jelier et al., 2008), the term 'ubiquitination' was found to be the most strongly associated biomedical concept with OPMD-deregulated genes (**Table 1** and **Table S3**). A regression-based analysis using global test (GT) (Goeman et al., 2004), and an enrichment method using DAVID (Dennis, Jr. et al., 2003; Huang et al., 2009) revealed highly significant deregulation of ubiquitin-proteasome system (UPS)-related GO (Gene Ontology) categories and KEGG (Kyoto Encyclopedia of Genes and Genomes) pathways across species (**Table 1**).

To evaluate the level of concordance between the animal models and OPMD patients, gene overlap between the OPMD-deregulated UPS genes was determined. Homologous genes were annotated using the HomoloGene and Inparanoid databases (see Methods). In total, 16%, 32% and 25% of the genes annotated to the UPS were identified as OPMD-deregulated in *Drosophila*, mouse and human, respectively (**Figure 1A**). More than half of the OPMD-deregulated genes in *Drosophila* (59%) overlapped with their mouse or human homologous genes, and close to half (45% and 51%) overlapped between mouse and human genes, respectively (**Figure 1A**). The similarity of deregulation direction across species was demonstrated for 14 genes, for which probes were found in all organisms (**Figure 1B**). Similar transcriptional changes were found for 13 homologous genes in mouse and human datasets. Among those, 8 genes showed similar changes in *Drosophila.* These results show the consistent UPS deregulation in OPMD.

To validate the microarray analyses, quantitative RT-PCR (Q-PCR) was performed on 19 OPMD-deregulated UPS genes from mouse. Genes were selected based on *P*-value and >1.3 fold change criteria. For 17/19 genes (89%), Q-PCR results confirmed the results of the microarray analyses (**Figure S2**). This demonstrates the reproducibility and validity of the microarray statistical analyses.

In the A17.1 mouse model, muscle atrophy is more prominent in fast glycolytic fibers (quadriceps) as compared with slow oxidative fibers (soleus) (Trollet et al., 2010). Since muscle atrophy is regulated by the UPS (Cao et al., 2005; Bodine et al., 2001; Sandri, 2008), we analyzed the muscle-

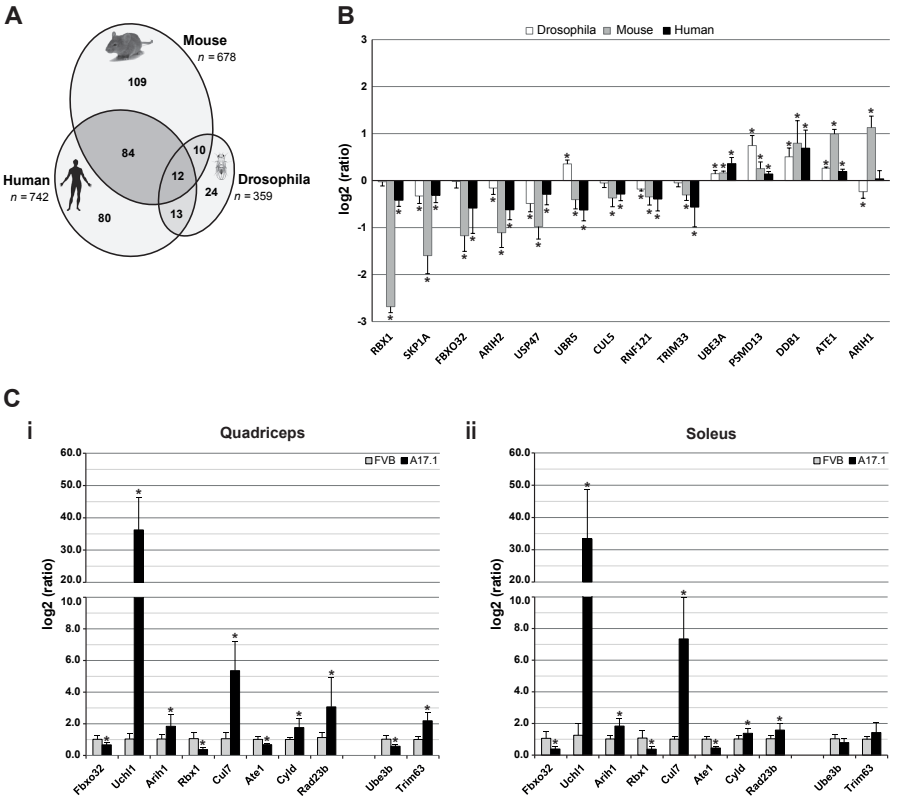

Figure 1 - Cross species deregulation of ubiquitin-proteasome in OPMD. A) Venn-diagram displaying the overlap in OPMD-deregulated genes in UPS across species. In mouse and *Drosophila*, OPMD-deregulated genes should be consistently deregulated in at least two time points. The total number of genes in UPS is indicated in italics. The list of OPMD-deregulated UPS genes is in Additional File 1. **B)** Transcriptional changes of selected genes in UPS in different organisms. Histograms display the log2(ratio) of the measured expression values in *Drosophila* (white bars), mouse (gray bars), and human (black bars). Significant changes with the adjusted $P < 0.05$ are indicated by ∗. **C)** RT Q-PCR validation of selected deregulated genes in UPS was carried out on quadriceps (**i**) and soleus (**ii**) muscles of 6 week-old mice. Histograms show the measured expression values for A17.1 and FVB mice using Q-PCR. Significant changes of measured expression values of A17.1 mice as compared to FVB with the $P < 0.05$ are indicated by ∗.

type specific expression of 10 OPMD-deregulated UPS genes in order to identify a correlation with muscle atrophy. Q-PCR was performed on RNA isolated from quadriceps and soleus of 6 week-old A17.1 and control (FVB) mice. The majority (8 out of 10) of genes showed no fiber-type specificity (**Figure 1C**). Only the deregulation of *Trim63* (Trollet et al., 2010) and *Ube3b* were specific to fast glycolytic fibers (**Figure 1C**). This suggests that the majority of OPMD-deregulated UPS genes are not associated with muscle atrophy in the A17.1 mouse.

The UPS involves an enzymatic cascade of ubiquitination and degradation steps. The ubiquitination steps start with ubiquitin activation, which requires the ubiquitin-activating enzyme (E1) and ubiquitin (Ub). This process results in the binding of Ub to the E2-conjugating enzyme. In a subsequent step the target protein is ubiquitinated with Ub-E2 and E3-ligase complexes, which ensures target specificity. Poly-ubiquitinated proteins are subjected to degradation. This

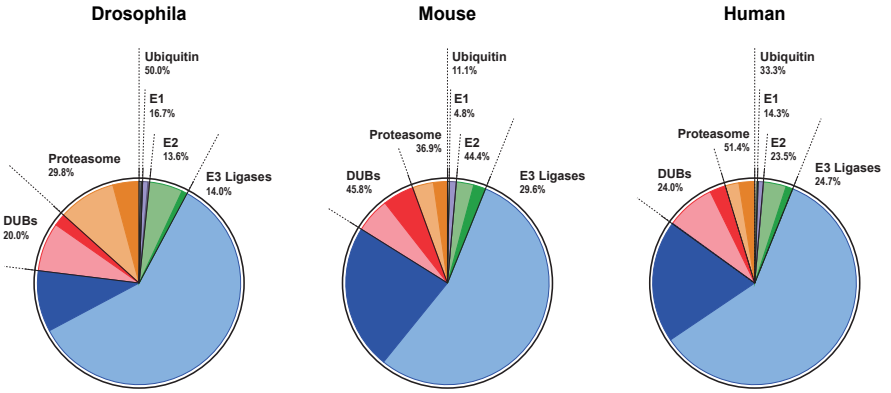

Figure 2 - Pie charts show the relative distribution of the UPS units (light colors) and OPMD-deregulated genes (dark colors) per organism. Numbers indicate the percentage of OPMD-deregulation.

step is employed by the deubiquitinating enzymes (DUBs) and the proteasome (Reyes-Turcu et al., 2009; Finley, 2009). Deregulation of genes involved in the ubiquitin activation step was not found to be consistent between OPMD and the models (**Figure 2** and **Table 2**). Ubiquitin up-regulation was previously reported in a non-muscle cell model for OPMD (Abu-Baker et al., 2003). Our study identified only one ubiquitin-encoding gene to be up regulated in mouse and human genomes, but these deregulated genes were not consistent across species. The E2-conjugating enzymes were significantly deregulated in *Drosophila* and mouse genomes, whereas in humans, the *P*-value for these enzymes was not significant. This suggests a weak association of E2 deregulation with OPMD (**Figure 2** and **Table 2**). In contrast, consistent deregulation was found for E3-ligases, DUBs, and proteasome (**Figure 2** and **Table 2**). The significance of this strong association was further evaluated by gene-overlap of homologous genes in human and mouse (**Table 2**). The gene overlap between mouse and human was found to be significant for all these three UPS components (*P*-values are 6.64E-08 for E3-ligases, 1.37E-02 for DUBs and 1.70E-02 for the proteasome). Overall, this analysis demonstrates consistent deregulation of E3-ligases, DUBs and proteasome across species.

OPMD is characterized by a late onset and a slow progression of muscle weaknesses (VICTOR et al., 1962; Brais et al., 1998). Progressive muscle weakness has also been reported in the mouse model (Davies et al., 2005). In 6 week-old mice symptoms were not detected, while muscle weakness was present in 18 week-old mice and was more pronounced by 26 weeks (Davies et al., 2005). If changes in expression levels are associated with disease onset and progression, a correlation between age and expression levels should be expected. A linear regression model was applied to the mouse UPS genes at three time points in order to identify genes that their expression trends are progressively changed. 80% of the OPMD-deregulated UPS genes show a progressive trend, which is age-associated (N=171/217, **Figure S3A,** examples for progressive expression trends are shown in **Figure 3Ai**). To identify genes with expression trends that are specific to the disease a regression model that combines age and disease features was applied. In 30% of the age-associated OPMD-deregulated UPS genes (N=50, **Figure S3B)** the progression trends significantly (*P*-value<0.05) differed between A17.1 and the wild-type (WT) controls (examples for progressive expression trends are shown in **Figure 3Bi**). The genes with disease-specific progression can be used to mark disease progression and could contribute to disease onset and progression. The

Table 2 - The distribution of OPMD-deregulated genes in UPS functional units and protein degradation categories. The number of annotated genes per unit, the percentage of OPMD-deregulated (D.E.) genes and *P*-values are indicated per organism. For *Drosophila* and mouse statistics is generated in combined datasets from three time points. The overlap in OPMD-deregulated genes between human and mouse and the percentage of deregulated genes in human D.E. genes are indicated. Protein degradation machineries are depicted by ¥.

	Drosophila		Mouse		Human		Overlap mouse vs. human	
	% D.E. Genes	P-Value (FDR)	% D.E. Genes	P-Value (FDR)	% D.E. Genes	P-Value (FDR)	# D.E. Genes	% D.E. Genes
Ubiquitin	50.00	4.18E-05	11.11	1.28E-01	33.33	1.19E-01	0	00.00
E1 Ubiquitin Activation	16.67	1.24E-01	04.76	7.29E-02	14.29	7.94E-02	0	00.00
E2 Ubiquitin Conjugation	13.64	9.19E-06	44.42	1.51E-08	23.53	7.31E-02	3	37.50
E3 Ubiquitin Ligase	13.99	1.92E-04	29.58	1.64E-08	24.74	4.35E-03	69	47.59
Deubiquitination (DUB)	20.00	1.63E-05	45.83	1.48E-08	24.00	3.15E-02	13	72.22
¥ Proteasome	29.79	2.15E-04	36.94	1.37E-07	51.35	9.27E-03	11	57.90
¥ Autophagy	25.00	1.07E-03	30.77	8.13E-08	18.75	1.37E-02	1	16.67
¥ Lysosome	5.00	1.64E-02	25.33	6.06E-03	24.68	1.54E-02	6	33.33

group of genes whose expression changes with age independent from the disease, however, may contribute to the late onset of the disease.

The vast majority of OPMD-deregulated UPS genes, which exhibit progressive expression profiles encode for E3-ligases (**Figure S3**). Expression trends for selected E3-ligases are presented in Figure 3. Confirmation of the analysis in mouse was carried out on the human homologues (**Figure 3**). The age-associated expression trends were similar between A17.1 and WT in mouse and between controls and expPABPN1 carriers at pre-symptomatic and symptomatic stages in human (**Figure 3A**). The progression trends did not significantly differ between genotypes (*P*-value > 0.05). In contrast, for those genes with expression trends associated with age and disease the expression trends of controls significantly differed from those of OPMD subjects (**Figure 3B**, *P*-value <0.05). Validation of progression analysis was performed by Q-PCR analysis of RNA from 6 and 26 week-old mice (**Figure 3C**). The Q-PCR results demonstrate the reproducibility and validity of the microarray progression analysis.

In the progression analysis some differences between human and mouse were noted. The progression of *Trim63* is mouse-specific, whereas the expression of the human *TRIM63* is not age-associated or OPMD-deregulated (**Figure 3B)**. *Asb11* is down regulated in mouse while it is up regulated in human (**Figure 3A**). The expression trend of *Socs4* in mouse is negative while in human it is positive (**Figure 3B**). These discrepancies could reflect differences between the two organisms or between the heterozygous and the high over-expression situation.

Expression of expPABPN1 leads to INI formation in affected muscles (Davies et al., 2005; Trollet et al., 2010). Previous studies have demonstrated that ubiquitin and proteasome proteins co-localize with INI in affected muscles (Calado et al., 2000) and in non-muscle cells (Abu-Baker et al., 2003; Tavanez et al., 2005). Since INI formation is a hallmark of OPMD, we studied whether the expression profiles of OPMD-deregulated E3-ligases correlate with their entrapment with expPABPN1 in INI. Co-localization was analyzed with an immunofluorescence procedure in C2C12 myotubes expressing expPABPN1 fused to yellow fluorescent protein (YFP). From the

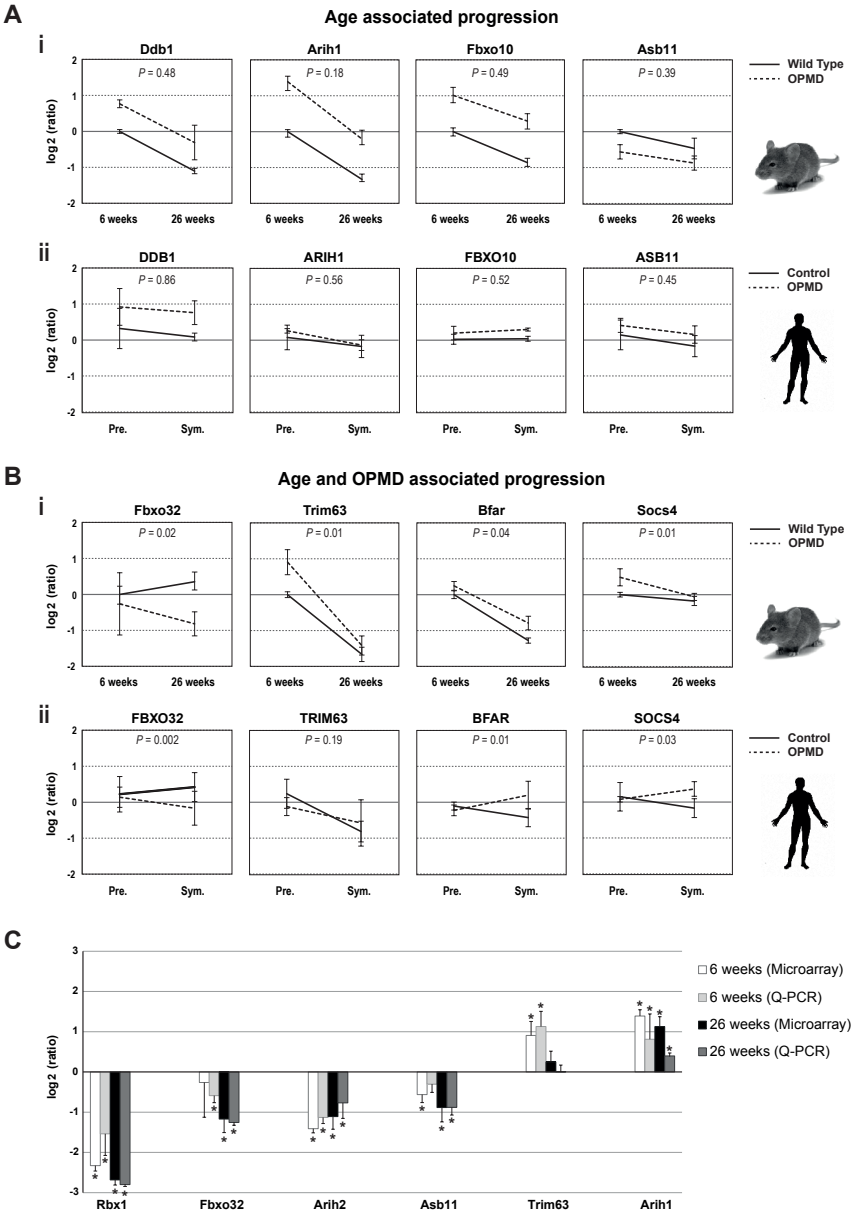

Figure 3 - Progressive changes in UPS gene expression. Progression trends for selected genes in mouse (**i**) and human (**ii**). Expression values were normalized to 6 weeks-old WT in mouse, and to young healthy controls (19 years-old in average) in human. *P*-values demonstrate the significance of differences in expression trends between controls and OPMD samples. **A)** The age-associated progression trend is indicated by *P*-value >0.05. **B)** The genotype-specific progression trend is indicated by *P*-values <0.05. SD represents variations in mouse (6 weeks N=5 and 26 weeks N=6) and in human (expPABPN1 carriers N=4 and controls N=5). **C)** RT Q-PCR validation of selected deregulated genes in UPS was carried out on skeletal muscles of 6 week-old and 26 week-old mice. Histograms show the log2(ratio) of the measured expression values using microarray and Q-PCR. Significant changes with the $P < 0.05$ are indicated by ∗.

E3-ligases encoding genes that showed an association with disease onset or progression (**Figure 3**), five were selected for co-localization studies using specific antibodies recognizing single proteins at the appropriate molecular weights. All 5 proteins showed nuclear localization in myotubes and co-localized with expPABPN1 in INI (**Figures 4**). Arih1, Asb11 and Ddb1 co-localized with all sizes of INI structures (**Figure 4A**) while the co-localization of Trim63 and Fbxo32 proteins were only evident for larger INI structures (**Figure 4B**, highlighted in boxes). This suggests a correlation between changes in expression trends and temporal entrapment in INI.

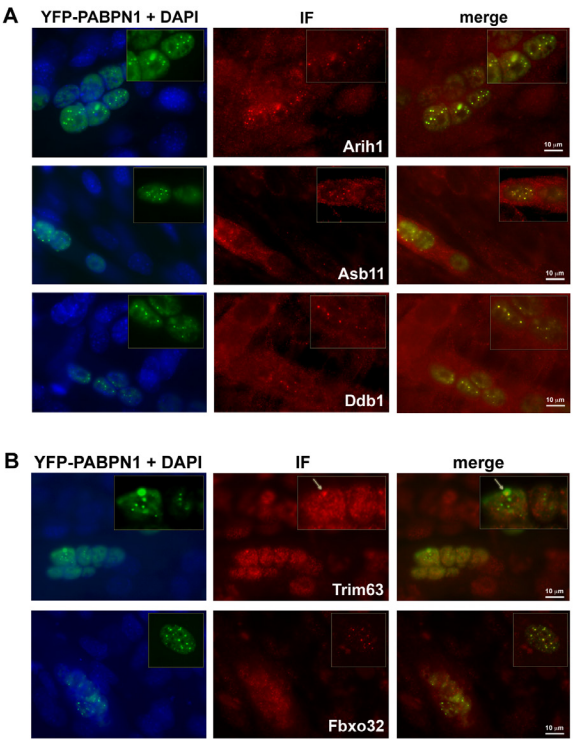

Figure 4 - Co-localization of selected E3 ligases with INI in C2C12 myotubes expressing YFP-Ala16PABPN1. Immunostaining of E3-ligases was visualized with Alexa-594 secondary antibodies. Co-localization with expPABPN1 in myotubes is demonstrated in the merge image. A 2.5X magnification of nuclei containing expPABPN1 aggregates is highlighted in a box. **A)** Arih1, Asb11 and Ddb1 E3 ligases show consistent co-localization with aggregated YFP-Ala16-PABPN1. **B)** Trim63 and Fbxo32 E3 ligases show progressively more co-localization with YFP-Ala16-PABPN1 as INI size increases. Scale bar is 10μm.

The proteasome is composed of core and regulatory subunits. Genes encoding for the proteasome core subunit were prominently down regulated in mouse and human (66% and 75%, respectively), while no preference in deregulation direction was found for the regulatory subunit (**Figure 5A** and **Table S5**). Down-regulation of the proteasome could affect protein degradation and, hence, protein accumulation. In C2C12 myoblasts that were treated with low concentrations (5 μM) of the proteasome inhibitor MG132, the accumulation of expPABPN1 was significantly higher as compared with mock-treated cells (**Figure 5B**). Similarly, treatment with the DUB inhibitor, PR619, also caused expPABPN1 accumulation (**Figure 5B**). High nuclear accumulation of expPABPN1, which accompanies INI formation, was consistently measured in MG132 treated cells using a cell-based intensity fluorescence quantification assay (**Figure 5C**). Thus, reduced proteasome and DUB activities in muscle cells promoted expPABPN1 accumulation and INI formation in muscle cells. However, expPABPN1 accumulation stimulated by proteasome inhibition is not specific to muscle cells (Abu-Baker et al., 2003).

In addition to the proteasome, the lysosome and the autophagy machineries can also facilitate protein catabolism. To evaluate whether one of these machineries could also regulate expPABPN1 protein accumulation the significance of deregulation in OPMD was analyzed. Overall, deregulation of lysosome and autophagy were not consistent across species. The lysosome KEGG pathway was evaluated as significantly deregulated in OPMD across species by GT but not by DAVID analysis (**Table 2**). However, in the literature-aided analysis, only a low level of association was found between OPMD-deregulated genes and lysosome in *Drosophila* and human

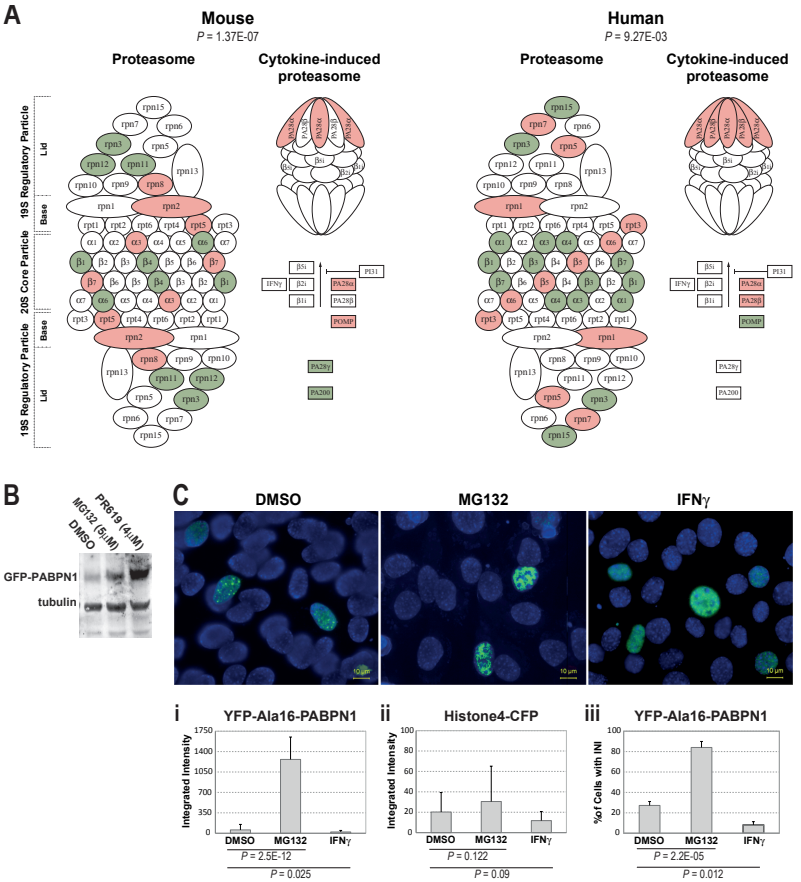

Figure 5 - The effect of altered proteasome activity on expPABPN1 accumulation and aggregation. **A)** Substantial deregulation of proteasome and immunoproteasome encoding genes in mouse and human. Down-regulation (green) is more pronounced in the core subunit of the proteasome. Immunoproteasome shows consistent up-regulation (red) in both organisms. **B)** Western blot analysis of YFP-Ala16-PABPN1 transfected C2C12 cells that were treated with 5μM MG132 or 5nM PR619. Control cells were treated with DMSO. **C)** Images show YFP-Ala16-PABPN1 localization in C2C12 after mock-treatment (DMSO), 5 μM MG132 or 5U/ml IFNγ. Scale bar equals 10 μm. Histograms show the integrated intensity of YFP-Ala16-PABPN1 (**i**) or Histone4-CFP (control) (**ii**), and the percentage of cells with INI in YFP-Ala16-PABPN1 expressing cells (**iii**). Averages represent 509, 773 and 476 cells for DMSO, MG132 and IFNγ, respectively. Significant difference between treatments is reflected by *P*-values.

(ranked at positions 196 and 789, respectively), while no association was found in mice. Similarly, the autophagy KEGG pathway was significant across species based on GT but not on DAVID analysis (**Table 2**). In the literature-aided analysis, autophagy was ranked 12 in mice, but a lower priority (ranked 136 and 154) was found in *Drosophila* and humans, respectively. Furthermore, the OPMD-deregulated gene overlap between mouse and human were not significant for either lysosome or autophagy pathways (*P*-values: 5.37E-01 and 3.70E-01, respectively). This is in sharp contrast to the consistent proteasome deregulation found across species. This indicates that, from the protein degradation pathways, only proteasome deregulation is consistently associated with OPMD across species. From this analysis we cannot exclude lysosome or autophagy deregulation in OPMD, but the lack of consistency across species and in three bioinformatics analyses suggests a smaller contribution as compared with the proteasome.

In contrast to the down regulation of genes in the core-subunit, the expression of genes encoding for the immunoproteasome subunit (the cytokine-induced proteasome) was consistently elevated in OPMD (**Figure 5A**). The immunoproteasome was initially identified in cells of the immune system after cytokine induction, which is involved in MHC-class-I antigen presentation (Kloetzel and Ossendorp, 2004). However, the accumulation of cytokine-induced proteasome proteins was also found in aging skeletal muscle cells (Ferrington et al., 2005). Treatment of C2C12 myoblasts with IFNγ, an inducer of immunoproteasome activity (Osna et al., 2003), led to a significant reduction in nuclear expPABPN1 accumulation (**Figure 5C** and **5Ci**) and INI formation (**Figure 5Ciii**). In contrast to expPABPN1, accumulation of Histone4, which is also a nuclear protein, was not significantly affected by manipulation of proteasome activity (**Figure 5Cii**). This suggests that the accumulation of expPABPN1, but not of Histone4, is receptive to the level of proteasome and immunoproteasome activity. Together, our results demonstrate that the UPS degradation machinery regulates expPABPN1 accumulation.

DISCUSSION

UPS is a cellular regulator of homeostasis and is involved in a wide spectrum of human diseases including cancer, neurodegenerative disorders and diabetes (Hoeller and Dikic, 2009; Liu et al., 2000; Combaret et al., 2009; Taillandier et al., 2004; Ciechanover and Brundin, 2003). Deregulation of UPS has been reported for myotonic dystrophy type 1 (Vignaud et al., 2010) and muscle atrophy in mice (Cao et al., 2005; Bodine et al., 2001; Sandri, 2008). In addition, altered UPS activity has been associated with muscle ageing (Combaret et al., 2009; Lee et al., 1999). Together these studies suggest that muscle cell function is tightly regulated by the UPS. In this study, we identified the UPS as the most consistently and significantly deregulated cellular machinery in OPMD animal models and patients. Transcriptome studies in non-muscle cells expressing expPABPN1 did not reveal substantial and predominant deregulation of UPS genes (Corbeil-Girard et al., 2005). This indicates that the effect of expPABPN1 on UPS deregulation is specific to muscle cells. Since PABPN1 is ubiquitously expressed in every cell but the phenotype is limited to muscle cells this suggests that UPS deregulation confers the muscle-specific pathogenesis of OPMD.

From six UPS components, only E3-ligases, DUBs and the proteasome were found to be consistently and prominently deregulated in OPMD across species. Relevant to OPMD proteasome activity is reduced during muscle aging (Combaret et al., 2009; Lee et al., 1999; Ferrington et al., 2005), and is associated with transcriptional deregulation of proteasomal genes (Lee et al., 1999). In the analysis of expression trends the expression of 89% of the OPMD-deregulated proteasome genes were found to be age-associated. This suggests that the natural decrease in proteasome expression during muscle aging can contribute to the late onset of the disease. Our analysis revealed that the core subunit of the proteasome is the only UPS subunit that was consistently down regulated which can cause reduced activity of the proteasome machinery. In a recent study, we found that expression of expPABPN1 in myotubes leads to down-regulation of proteasome-encoding genes, and causing the accumulation of expPABPN1 protein (unpublished data). However, proteasome regulation of expPABPN1 accumulation and INI formation is not specific to muscle cells (Abu-Baker et al., 2003). Since in patients INI are formed only in muscle cells this suggests that proteasome down-regulation during muscle aging triggers expPABPN1 accumulation. In turn, accumulation of expPABPN1 leads to extensive proteasome down-regulation in OPMD (**Figure 6**). This feed forward model could justify the muscle-specific INI formation and the late onset in OPMD.

Hypothesizing that changes in expression levels could reflect pathological changes in disease sta-

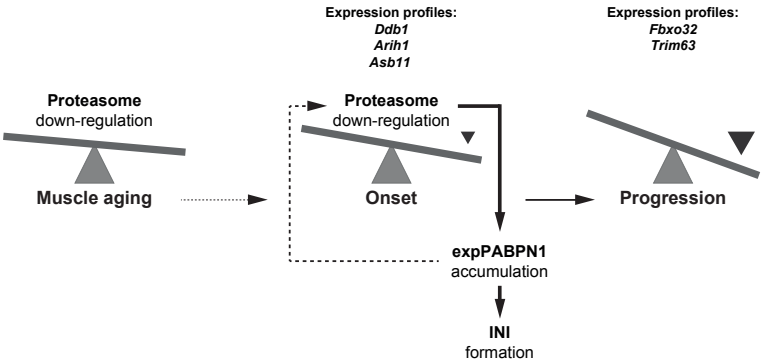

Figure 6 - A model for the involvement of UPS in OPMD disease pathology. In muscle, age-associated proteasome down regulation affects expPABPN1 protein accumulation. Elevated expPABPN1 accumulation affects proteasome deregulation during disease onset. Expression profiles of E3-ligases can be sued to separate disease onset from progression.

tus we have studied the correlation between transcriptional changes of OPMD-deregulated UPS genes and age. Noticeably, the expression of the vast majority of the OPMD-deregulated UPS genes is progressed during normal muscle aging. This suggests that transcriptional changes of these genes are associated with disease onset. The expression trends of a subset of these genes showed disease-specific progression. Among those, *Trim63* and *Fbxo32* exhibited disease progression in mouse. Both genes are known for regulating muscle atrophy in mice (Cao et al., 2005; Bodine et al., 2001; Sandri, 2008). In the OPMD mouse model, muscle atrophy in exhibited only in fast muscle glycolytic fibres and *Trim63* expression correlates with muscle atrophy in A17.1 (Trollet et al., 2010). However, the majority of the OPMD-deregulated UPS genes did not show fibre-type specific expression. This could suggest that UPS deregulation in OPMD has a broader pathological effect than muscle atrophy. Indeed, in affected muscles of OPMD patients, atrophy may be evident only at a later stage of disease progression. Although a high degree of consistency between expression trends in mice and human was found for the majority of the genes analyzed in this study. *Trim63* deregulation and progression is probably mouse-specific, as OPMD-deregulation or progression was not found in human. *Fbxo32,* however, was consistently deregulated in both organisms and, therefore, can be a candidate for regulating disease progression and muscle atrophy in human. After mining the NCBI dataset for tissue-specific expression (Unigene Hs.352183, Build No. 228 released 2010), *Asb11* was noted for its specific expression in skeletal muscles**.** Since *Asb11* is consistently OPMD-deregulated in human and mouse, and its expression trend is associated with disease onset it could represent a relevant candidate for functional genomic studies. This shows that cross-species transcriptome and progression analyses can be used to identify target molecules for future studies.

OPMD is characterized by INI formation. The role of INIs in disease pathogenesis is unknown. Previous studies have shown that many genes whose expression is deregulated by expPABPN1 are found to be co-localized in INI (Corbeil-Girard et al., 2005). Components of the proteasome, which is OPMD-deregulated, also co-localize in INI (Abu-Baker et al., 2003; Tavanez et al., 2005). We also found that many of the OPMD deregulated E3-ligases are entrapped in INI. Moreover, we demonstrate a correlation between temporal changes in expression levels and sequential entrapment in INI. Together these studies suggest that entrapment in INI could lead to transcriptional deregulation. It is possible that protein entrapment in INI affects gene expression through a compensatory mechanism resulting in altered transcriptional profiles.

CONCLUSIONS

In this study, we combined expression datasets from three organisms and disease models with different bioinformatics analyses in a single study. This allowed us to identify with high confidence the UPS as the most predominantly deregulated cellular pathway in OPMD. This approach differs from most microarray studies where results are derived from a single computational analysis performed on a single organism. We show that with this combined bioinformatics approach the list of deregulated pathways can be prioritized with high confidence. This approach can facilitate studies with complex biological situations and massive gene deregulation such as late onset disorders and rare-diseases.

The most significant and novel finding in this study is the substantial and cross-species consistent deregulation of the ubiquitin-proteasome system (UPS) in OPMD. We propose that protein entrapment in PABPN1 aggregates is associated with a substantial transcriptional deregulation of the UPS that, in turn leads to disruption of homeostasis in skeletal muscles. By taking advantage of the detailed analysis of gene expression trends and muscle- expression, we predict that candidate genes can be selected for functional genomic studies which ultimately lead to the identification of OPMD pathogenesis.

METHODS

Generation of microarray datasets

Drosophila and mouse microarray datasets have previously been published (Chartier et al., 2009; Trollet et al., 2010). Human quadriceps muscle samples were collected with the needle or by an open surgical procedure from OPMD patients and family members as well as from anonymous age-matching healthy individuals that gave informed consent. The presence of expansion mutation in PABPN1 in OPMD patients and pre-symptomatic was determined with sequencing. Bergstrom needle biopsies from the (pre)symptomatic patients were approved by the ethical committee. Total RNA was extracted from skeletal muscles using RNA Bee (Amsbio) according to the manufacturer's instructions. RNA integration number (RIN) was determined with RNA 6000 Nano (Agilent Technologies). RNA with RIN >7 were used for subsequent steps. RNA labeling was performed with the Illumina® TotalPrep RNA Amplification kit (Ambion) according to the manufacturer's protocol, and subsequently was hybridized to Illumina Human v3 Bead arrays. The generated microarray datasets are deposited and publicly available at GEO repository. GEO accession numbers for mouse and human microarray datasets are GSE26604 and GSE26605, respectively.

Data processing and statistical analysis

Microarray measurements were normalized using the quantile method (Smyth and Speed, 2003). Each organism and time point was normalized separately. The quality of the data was assessed by principal component analysis.

For *Drosophila* and mouse, genes differentially expressed between OPMD and control subjects were identified at each time point by applying a hierarchical linear model using the limma package in R (Smyth, 2004). Human subjects were grouped into healthy, pre-symptomatic and symptomatic subjects. *P*-value cut-offs of 0.05 after multiple-testing correction using the method of Benjamini and Hochberg (False Discovery Rate (FDR) were applied to the *Drosophila* and mouse samples and, due to higher inter-individual variation, a nominal *P*-value cut-off of 0.05 was used for human samples) were used. This resulted in lists of OPMD-deregulated genes for each time point and organism. Probe annotation was done using the indac (*Drosophila*), illuminaMousev-

1BeadID (mouse), and illuminaHumanv3BeadID (human) R packages. The OPMD significantly deregulated genes in the UPS from human and mouse datasets are listed in Additional File 1.

Pathway analyses

Global test (GT) (Goeman et al., 2004) was used to identify significant associations between GO categories or KEGG pathways and OPMD, while including age as a confounder (*Drosophila* and mouse only). Gene sets with multiple testing adjusted (Holm's method) *P-value* < 0.05 were selected as significant. DAVID, a functional annotation clustering tool (Dennis, Jr. et al., 2003; Huang et al., 2009), was applied on a list of OPMD-deregulated genes and pathway redundancy was removed by clustering similar GO categories and pathways. In addition, biomedical concepts that are associated with OPMD-deregulated genes were identified using literature-aided mapping tool, Anni 2.0 (Jelier et al., 2008). The procedure was performed for each organism separately. Cross-species analyses were carried out on a group of homologous genes. *Drosophila* homologues of mouse and human genes were annotated using HomoloGene (*http://www.ncbi.nlm.nih.gov/* homologene) and Inparanoid *(http://inparanoid.sbc.su.se)* online databases. Integration of three time-points in *Drosophila* and mouse (**Table S1**) were used to identify OPMD-deregulated pathways across species (**Figure 1**). A recent annotation of E3 ligases (Li et al., 2008) was used to identify OPMD-deregulated E3 ligases. The annotation for all other UPS components is extracted from KEGG. Since the annotation for genes encoding for lysosome is not available in R packages, we have extracted the annotation from KEGG website and integrated it into our pathway analyses.

Progression studies

For testing the significance of the association of expression trends of OPMD-deregulated genes with age, using limma model in R (Smyth, 2004), a linear regression model ($expression \sim \alpha OPMD + \beta AGE + \delta(OPMD \times AGE) + \varepsilon$) was applied on combined datasets from 6 and 26 weeks old mice. Age-associated changes were identified as those with β significantly different from zero. OPMD- and age-associated changes were defined as those with δ significantly different from zero. To determine whether the expression profiles of individual genes significantly differ between controls and OPMD *P*-values are FDR-corrected with the cut-off threshold of 0.05.

Quantitative RT-PCR analysis

Primers for Q-PCR validation were designed in the sequence surrounding the Illumina probe location using Primer 3 plus program. RT-QPCR was performed according to the procedure in Trollet et al. (2010). The list of primers is provided in Table 3.

Cell culture and transfection

C2C12 cells were used for transient transfection experiments. C2C12 cells were cultured in DMEM containing 20% fetal calf serum. Prior to transfection, cells were seeded on glass. Transfection was carried out in 80% cell confluence with Lipofectamine™ 2000 (Invitrogen) according to the manufacturer's protocol. Plasmids used for transfection are YFP-Ala16-PABPN1 and Histone4-CFP. For the proteasome modification treatments, cells were treated 16 hours after transfection with DMSO (1:1000), 5 μM MG132 (Sigma-Aldrich), or 5U/ml IFNγ (HyCult Biotech) for 20 hours.

Protein detection and Imaging

For immunocytochemistry, 16 hours post-transfection with YFP-Ala16-PABPN1, C2C12 cells were incubated with fusion medium (DMEM supplemented with 2.5% Horse serum) for 2 days, and immunocytochemistry was performed after a short fixation (Raz et al., 2006) followed by a

15 min incubation with 1% Triton X100, during which PABPN1 aggregates remain intact. Following antibody incubations, preparations were mounted in Citifluor (Agar Scientific) containing 400 μg/ml of DAPI (Sigma-Aldrich). Immunofluorescent specimens were examined with a fluorescence microscope (Leica DM RXA), 63X and 100X lens NA 1.4 plan Apo objective. Integrated intensity was measured with ImageJ (http://rsbweb.nih.gov/ij/), and intensity values were corrected for background.

Antibodies used in this study are: Goat anti-Asb-11 (K16) (1:1000) Santa Cruz Biotechnology; Rabbit anti-atrogin-1 (1:1000) ECM Biosciences; Rabbit anti-Murf1 (1:1000) ECM Biosciences; Goat anti-DDB1 (1:1000) Abcam; mouse anti-Flag (1:2000) Sigma –Aldrich; Rabbit anti-Desmin MP Biomedicals. Alexa-Fluor 594 conjugated secondary (Invitrogen) or IRDye 680LT and 800CW conjugated secondaries (Licor Biosciences) were used to detection of first antibody.

Table 3 - The list of primers used for quantitative RT_PCR analysis.

Genes	Probe	FW Primer Sequence	RV Primer Sequence
Arih1	6900025	GAGAAGGATGGCGGTTGTAA	ATCTCTTGCTGCCTTTGCAT
Arih2	2810025	AGCCTAACTCCCCCTTGGTA	ACCACTGAGGGTGCAAAAAC
Ate1	6940722	CAAAGTGATTCTACTGTGGCTGA	ACGAAAATCTCCAATGCAGTC
Cul7	3360114	CGGGACTATGCGGTGATACT	GTGGGTTCGTCTGTGGTCTT
Psme3	2810537	GCGAAGGTCAAACCCATAGA	GAAAGTGATGCATCCCAGGT
Rbx1	2340047	TTGAGGCCAGCCTACAGAGT	AGGAAAACTCCCCTGAAGGA
Skp1a	2450102	TGCAGCTGGGCTCTCTTAAT	GTTTCTCCACCTGGGAACAA
Uchl1	1230066	CCTGTCCCTTCAGTTCCTCA	GATTAACCCCGAGATGCTGA
Huwe1	106840041	GCTGCATTGAGACTTGAAACC	TCCACAACACAGATGCCAAT
Tbl1x	6400524	ATTTTCCCCCTCCCCTAATC	GAGCCTGTTCTGGATGGAAA
Ube4b	3610154	GCTGGAGTGGATCAGGACTC	TGGTAAGGTCAAACCCCAAA
Ube2o	2190040	CGGTGAGCACATTACAGCTC	GCATCATGCTTTGGCTTTTT
Usp47	100940601	GAATGCTTGTAAAGTCCCGTTT	CTAGCACGCTCTGCAATGAA
Ppp2cb	5570593	ACTGCTACCGTTGTGGGAAC	AGGTCCTGGGGAGGAATTTA
Ube3b	6380458	GCCTGCACAGGTAACACAGA	ACCAGGAGCTGCTGAGATGT
Fbxo32	110037	GGGAGGCAATGTCTGTGTTT	AAGAGGTGCAGGGACTGAGA
Trim63	1740164	CGACCGAGTGCAGACGATCATCTC	GTGTCAAACTTCTGACTCAGC
Ubr5	1780605	GCTGCCTTTGTGGAAAGTGT	TTGCAGCCAACCACAAATAA
Asb11	2060487	TTGTGCTGAACAAGCTCCTG	GAGGGTCCTGAATCATCCAA
mHPRT	-	CGTCGTGATTAGCGATGATG	TTTTCCAAATCCTCGGCATA

Authors' contributions

SYA and AV preformed the bioinformatics studies. AV and VR preformed the molecular genetics studies. Biological samples were provided by: BS, BE, MS, JV, CT, GD, AC and MS. The manuscript was drafted by SYA and VR and written by SYA, PAC, SM and VR. PAC participated in the bioinformatics design, coordination and data analysis. All authors read and approved the manuscript.

Acknowledgement
This work was supported by grants from European Commission (PolyALA LSHM-CT-2005018675) and Muscular Dystrophy Association (68016) to S.M.M. and MDA, the Centre for Medical Systems Biology within the framework of the Netherlands Genomics Initiative (NGI)/Netherlands Organisation for Scientific Research (NWO), the CNRS (UPR1142), the ANR Genopat (ANR-09-GENO-025-01), the FRM ("Equipe FRM 2007" N°DEQ20071210560), and the European Commission (PolyALA LSHM-CT-2005-018675) to M.S. The funders had no role in study design, data collection and analysis, decision to publish, or preparation of the manuscript.

Reference List

Abu-Baker,A., Messaed,C., Laganiere,J., Gaspar,C., Brais,B., and Rouleau,G.A. (2003). Involvement of the ubiquitin-proteasome pathway and molecular chaperones in oculopharyngeal muscular dystrophy. Hum. Mol. Genet *12*, 2609-2623.

Blumen,S.C., Bouchard,J.P., Brais,B., Carasso,R.L., Paleacu,D., Drory,V.E., Chantal,S., Blumen,N., and Braverman,I. (2009). Cognitive impairment and reduced life span of oculopharyngeal muscular dystrophy homozygotes. Neurology *73*, 596-601.

Bodine,S.C., Latres,E., Baumhueter,S., Lai,V.K., Nunez,L., Clarke,B.A., Poueymirou,W.T., Panaro,F.J., Na,E., Dharmarajan,K., Pan,Z.Q., Valenzuela,D.M., DeChiara,T.M., Stitt,T.N., Yancopoulos,G.D., and Glass,D.J. (2001). Identification of ubiquitin ligases required for skeletal muscle atrophy. Science *294*, 1704-1708.

Brais,B., Bouchard,J.P., Xie,Y.G., Rochefort,D.L., Chretien,N., Tome,F.M., Lafreniere,R.G., Rommens,J.M., Uyama,E., Nohira,O., Blumen,S., Korczyn,A.D., Heutink,P., Mathieu,J., Duranceau,A., Codere,F., Fardeau,M., and Rouleau,G.A. (1998). Short GCG expansions in the PABP2 gene cause oculopharyngeal muscular dystrophy. Nat Genet *18*, 164-167.

Brais,B., Xie,Y.G., Sanson,M., Morgan,K., Weissenbach,J., Korczyn,A.D., Blumen,S.C., Fardeau,M., Tome,F.M., Bouchard,J.P., and . (1995). The oculopharyngeal muscular dystrophy locus maps to the region of the cardiac alpha and beta myosin heavy chain genes on chromosome 14q11.2-q13. Hum. Mol. Genet *4*, 429-434.

Calado,A., Tome,F.M., Brais,B., Rouleau,G.A., Kuhn,U., Wahle,E., and Carmo-Fonseca,M. (2000). Nuclear inclusions in oculopharyngeal muscular dystrophy consist of poly(A) binding protein 2 aggregates which sequester poly(A) RNA. Hum. Mol. Genet *9*, 2321-2328.

Cao,P.R., Kim,H.J., and Lecker,S.H. (2005). Ubiquitin-protein ligases in muscle wasting. Int. J. Biochem. Cell Biol. *37*, 2088-2097.

Catoire,H., Pasco,M.Y., Abu-Baker,A., Holbert,S., Tourette,C., Brais,B., Rouleau,G.A., Parker,J.A., and Neri,C. (2008). Sirtuin inhibition protects from the polyalanine muscular dystrophy protein PABPN1. Hum. Mol. Genet *17*, 2108-2117.

Chartier,A., Benoit,B., and Simonelig,M. (2006). A Drosophila model of oculopharyngeal muscular dystrophy reveals intrinsic toxicity of PABPN1. EMBO J *25*, 2253-2262.

Chartier,A., Raz,V., Sterrenburg,E., Verrips,C.T., van der Maarel,S.M., and Simonelig,M. (2009). Prevention of oculopharyngeal muscular dystrophy by muscular expression of Llama single-chain intrabodies in vivo. Hum. Mol. Genet.

Ciechanover,A. and Brundin,P. (2003). The ubiquitin proteasome system in neurodegenerative diseases: sometimes the chicken, sometimes the egg. Neuron *40*, 427-446.

Combaret,L., Dardevet,D., Bechet,D., Taillandier,D., Mosoni,L., and Attaix,D. (2009). Skeletal muscle proteolysis in aging. Curr. Opin. Clin. Nutr. Metab Care *12*, 37-41.

Corbeil-Girard,L.P., Klein,A.F., Sasseville,A.M., Lavoie,H., Dicaire,M.J., Saint-Denis,A., Page,M., Duranceau,A., Codere,F., Bouchard,J.P., Karpati,G., Rouleau,G.A., Massie,B., Langelier,Y., and Brais,B. (2005). PABPN1 overexpression leads to upregulation of genes encoding nuclear proteins that are sequestered in oculopharyngeal muscular dystrophy nuclear inclusions. Neurobiol. Dis. *18*, 551-567.

Davies,J.E., Sarkar,S., and Rubinsztein,D.C. (2006). Trehalose reduces aggregate formation and delays pathology in a transgenic mouse model of oculopharyngeal muscular dystrophy. Hum. Mol. Genet *15*, 23-31.

Davies,J.E., Wang,L., Garcia-Oroz,L., Cook,L.J., Vacher,C., O'Donovan,D.G., and Rubinsztein,D.C. (2005). Doxycycline attenuates and delays toxicity of the oculopharyngeal muscular dystrophy mutation in transgenic mice. Nat Med. *11*, 672-677.

Dennis,G., Jr., Sherman,B.T., Hosack,D.A., Yang,J., Gao,W., Lane,H.C., and Lempicki,R.A. (2003). DAVID: Database for Annotation, Visualization, and Integrated Discovery. Genome Biol. *4*, 3.

Fan,X. and Rouleau,G.A. (2003). Progress in understanding the pathogenesis of oculopharyngeal muscular dystrophy. Can. J. Neurol. Sci. *30*, 8-14.

Ferrington,D.A., Husom,A.D., and Thompson,L.V. (2005). Altered proteasome structure, function, and oxidation in aged muscle. FASEB J. *19*, 644-646.

Finley,D. (2009). Recognition and processing of ubiquitin-protein conjugates by the proteasome. Annu. Rev Biochem. *78*, 477-513.

Goeman,J.J., van de Geer,S.A., de,K.F., and van Houwelingen,H.C. (2004). A global test for groups of genes: testing association with a clinical outcome. Bioinformatics. *20*, 93-99.

Hino,H., Araki,K., Uyama,E., Takeya,M., Araki,M., Yoshinobu,K., Miike,K., Kawazoe,Y., Maeda,Y., Uchino,M., and Yamamura,K. (2004). Myopathy phenotype in transgenic mice expressing mutated PABPN1 as a model of oculopharyngeal muscular dystrophy. Hum. Mol. Genet *13*, 181-190.

Hoeller,D. and Dikic,I. (2009). Targeting the ubiquitin system in cancer therapy. Nature *458*, 438-444.

Huang,d.W., Sherman,B.T., and Lempicki,R.A. (2009). Systematic and integrative analysis of large gene lists using DAVID bioinformatics resources. Nat Protoc. *4*, 44-57.

Ioannidis,J.P., Allison,D.B., Ball,C.A., Coulibaly,I., Cui,X., Culhane,A.C., Falchi,M., Furlanello,C., Game,L., Jurman,G., Mangion,J., Mehta,T., Nitzberg,M., Page,G.P., Petretto,E., and van,N., V (2009). Repeatability of published microarray gene expression analyses. Nat Genet. *41*, 149-155.

Jelier,R., Schuemie,M.J., Veldhoven,A., Dorssers,L.C., Jenster,G., and Kors,J.A. (2008). Anni 2.0: a multipurpose text-mining tool for the life sciences. Genome Biol. *9*, R96.

Kloetzel,P.M. and Ossendorp,F. (2004). Proteasome and peptidase function in MHC-class-I-mediated antigen presentation. Curr. Opin. Immunol. *16*, 76-81.

Lee,C.K., Klopp,R.G., Weindruch,R., and Prolla,T.A. (1999). Gene expression profile of aging and its retardation by caloric restriction. Science *285*, 1390-1393.

Li,W., Bengtson,M.H., Ulbrich,A., Matsuda,A., Reddy,V.A., Orth,A., Chanda,S.K., Batalov,S., and Joazeiro,C.A. (2008). Genome-wide and functional annotation of human E3 ubiquitin ligases identifies MULAN, a mitochondrial E3 that regulates the organelle's dynamics and signaling. PLoS. One. *3*, e1487.

Liu,Z., Miers,W.R., Wei,L., and Barrett,E.J. (2000). The ubiquitin-proteasome proteolytic pathway in heart vs skeletal muscle: effects of acute diabetes. Biochem. Biophys. Res. Commun. *276*, 1255-1260.

Osna,N.A., Clemens,D.L., and Donohue,T.M., Jr. (2003). Interferon gamma enhances proteasome activity in recombinant Hep G2 cells that express cytochrome P4502E1: modulation by ethanol. Biochem. Pharmacol. *66*, 697-710.

Raz,V., Carlotti,F., Vermolen,B.J., van der,P.E., Sloos,W.C., Knaan-Shanzer,S., de Vries,A.A., Hoeben,R.C., Young,I.T., Tanke,H.J., Garini,Y., and Dirks,R.W. (2006). Changes in lamina structure are followed by spatial reorganization of heterochromatic regions in caspase-8-activated human mesenchymal stem cells. J Cell Sci. *119*, 4247-4256.

Reyes-Turcu,F.E., Ventii,K.H., and Wilkinson,K.D. (2009). Regulation and cellular roles of ubiquitin-specific deubiquitinating enzymes. Annu. Rev Biochem. *78*, 363-397.

Sandri,M. (2008). Signaling in muscle atrophy and hypertrophy. Physiology. (Bethesda.) *23*, 160-170.

Smyth,G.K. (2004). Linear models and empirical bayes methods for assessing differential expression in microarray experiments. Stat. Appl. Genet. Mol. Biol. *3*, Article3.

Smyth,G.K. and Speed,T. (2003). Normalization of cDNA microarray data. Methods *31*, 265-273.

Taillandier,D., Combaret,L., Pouch,M.N., Samuels,S.E., Bechet,D., and Attaix,D. (2004). The role of ubiquitin-proteasome-dependent proteolysis in the remodelling of skeletal muscle. Proc. Nutr. Soc. *63*, 357-361.

Tavanez,J.P., Calado,P., Braga,J., Lafarga,M., and Carmo-Fonseca,M. (2005). In vivo aggregation properties of the nuclear poly(A)-binding protein PABPN1. RNA. *11*, 752-762.

Tome,F.M. and Fardeau,M. (1980). Nuclear inclusions in oculopharyngeal dystrophy. Acta Neuropathol. *49*, 85-87.

Trollet,C., Anvar,S.Y., Venema,A., Hargreaves,I.P., Foster,K., Vignaud,A., Ferry,A., Negroni,E., Hourde,C., Baraibar,M.A., 't Hoen,P.A., Davies,J.E., Rubinsztein,D.C., Heales,S.J., Mouly,V., van der Maarel,S.M., Butler-Browne,G., Raz,V., and Dickson,G. (2010). Molecular and phenotypic characterization of a mouse model of oculopharyngeal muscular dystrophy reveals severe muscular atrophy restricted to fast glycolytic fibres. Hum. Mol. Genet.

VICTOR,M., HAYES,R., and ADAMS,R.D. (1962). Oculopharyngeal muscular dystrophy. A familial disease of late life characterized by dysphagia and progressive ptosis of the evelids. N. Engl. J. Med. *267*, 1267-1272.

Vignaud,A., Ferry,A., Huguet,A., Baraibar,M., Trollet,C., Hyzewicz,J., Butler-Browne,G., Puymirat,J., Gourdon,G., and Furling,D. (2010). Progressive skeletal muscle weakness in transgenic mice expressing CTG expansions is associated with the activation of the ubiquitin-proteasome pathway. Neuromuscul. Disord. *20*, 319-325.

APPENDIX

Supplementary Table 1A - Overview of genome-wide transcriptome microarray datasets of *Drosophila* and mouse OPMD models and muscle biopsies of OPMD patients.

Biological Systems	Tissue	Number of Samples		Age	MA Platform
Drosophila	Adult thoracic muscles	3	pools of 50 flies per genotype	1 day 6 days 11 days	15K INDAC spotted oligonucleotide array
Mouse	Quadriceps	6	replicates per genotype	6 weeks 18 weeks 26 weeks	Illumina 48K Mouse v.1 bead array
Human	Quadriceps	9 13 39	Pre-symptomatic Symptomatic Controls	17 – 22 years control 31 – 40 years Pre-Symptomatic 38 – 42 years control 49 – 60 years symptomatic 58 – 67 years control	Illumina 48K Human v.3 bead array

Supplementary Table 1B - Overview of muscle biopsies of OPMD patients and controls. All patients are heterozygous expPABPN1 carriers as indicated by sequence analysis.

	Sex	Age	GCG Mutation	Muscle Histology
Pre-Symptomatic	Female	39	12/6	Sporadic atrophic fibre
	Female	37	10/6	Moderate dystrophic alterations
	Female	37	12/6	Normal
	Female	31	9/6	Slight dystrophic alteration
Symptomatic	Female	60	9/6	Moderate dystrophic alterations
	Female	49	10/6	Moderate dystrophic alterations
	Male	59	10/6	Moderate dystrophic alterations
	Female	57	11/6	Severe dystrophic alterations

Supplementary Figure 1 - Integrated cross-species high-throughput transcriptome study.

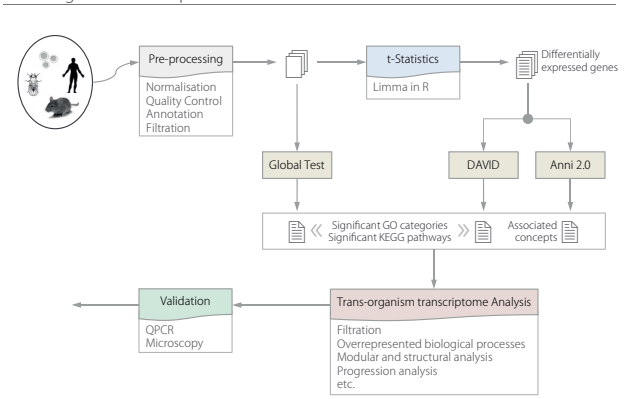

Supplementary Table 2 - Literature-aided analysis of the association of biomedical concepts with OPMD-deregulated genes.

	Drosophila		Mouse		Human
1	ribosomal protein activity	1	Ubiquitination	1	ubiquitin activity
2	ubiquitin activity	2	Ubiquitins	2	RNA Binding
3	RNA Binding	3	Ubiquitin	3	Ubiquitination
4	Ubiquitination	4	Ligase	4	RNA Splicing
5	polyethylene glycol monostearate	5	SNAP receptor	5	GTP Binding
6	Ligase	6	Internal Ribosome Entry Site	6	protein transport
7	POLR2F	7	Phosphotransferases	7	Alternative Splicing
8	GTP Binding	8	Cullin Proteins	8	Transcription, Genetic
9	ribosome biogenesis and assembly	9	Muscle Proteins	9	intracellular protein transport
10	Ribosome Subunits	10	Mitogen-Activated Protein Kinases	10	GTP-binding

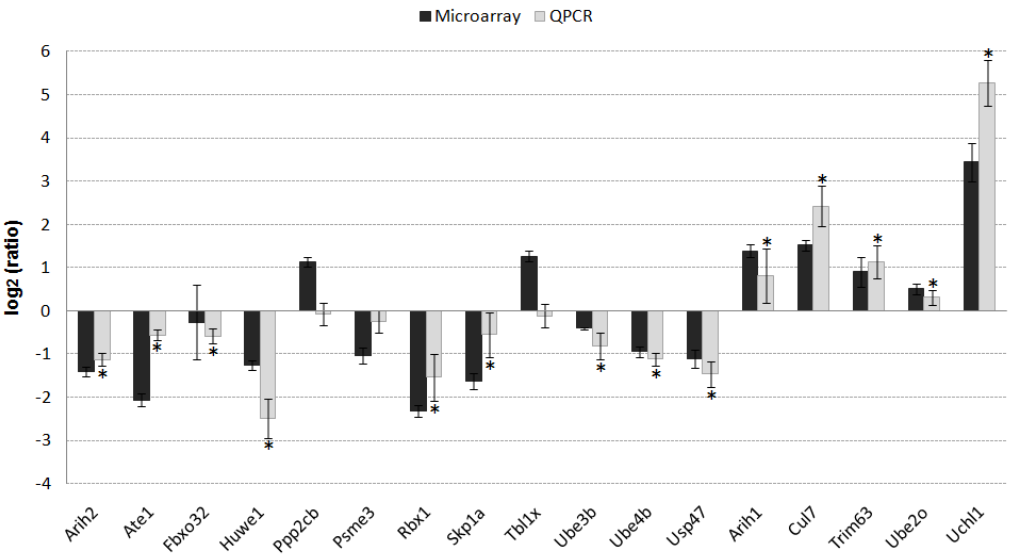

Supplementary Figure 2 - Validation of expression level of selected genes from the pool of UPS OPMD-deregulated genes on the skeletal muscle of 6 weeks-old OPMD mice, normalized to WT. Histograms indicate the log2(ratio) of the measured expression values using RT Q-PCR (grey bars) and microarray (black bars) for 4 WT and 6 OPMC mice (∗ P <0.05).

Supplementary Table 3 - Spreading of OPMD-deregulation in UPS over the functional components and sub-classes of E3-ligases. The number of total genes in each component is shown; the percentage of OPMD-deregulated (D.E.) genes and *P*-values are indicated. For *Drosophila* and mouse, *P*-values indicate the significance of OPMD-deregulation in combined datasets from three time-points and the percentage of D.E. genes represents an average across three time-points. The overlap in OPMD-deregulated genes between human and mouse is shown and the percentage of deregulated genes shows the fraction of overlap in human D.E. genes.

										Overlap	
	Drosophila			Mouse			Human			Mouse vs. Human	
	# Total Genes	% D.E. Genes	*P*-Value (FDR)	# Total Genes	% D.E. Genes	*P*-Value (FDR)	# Total Genes	% D.E. Genes	*P*-Value (FDR)	# D.E. Genes	% D.E. Genes
Ubiquitin	2	50.00	4.18E-05	3	11.11	1.28E-01	3	33.33	1.19E-01	0	00.00
E1 Ubiquitin Activation	4	16.67	1.24E-01	7	04.76	7.29E-02	7	14.29	7.94E-02	0	00.00
E2 Ubiquitin Conjugation	22	13.64	9.19E-06	33	44.42	1.51E-08	34	23.53	7.31E-02	3	37.50
E3 Ubiquitin Ligase	249	13.99	1.92E-04	526	29.58	1.64E-08	586	24.74	4.35E-03	69	47.59
RING	226	13.61	1.29E-04	495	28.13	1.67E-08	550	23.04	7.83E-03	60	47.35
HECT	16	22.92	2.49E-02	23	42.00	1.68E-08	28	32.14	1.59E-02	7	77.78
U-Box	7	4.76	6.98E-01	8	46.00	2.52E-08	8	37.50	7.94E-03	2	66.67
Deubiquitination (DUB)	35	20.00	1.63E-05	72	45.83	1.48E-08	75	24.00	3.15E-02	13	72.22
Proteasome	47	29.79	2.15E-04	37	36.94	1.37E-07	37	51.35	9.27E-03	11	57.90

Supplementary Table 4 - Direction of OPMD-deregulation over the functional components of UPS that are significantly deregulated in all organisms.

	Mouse				Human			
	# Total Genes	% D.E. Genes	UP	DOWN	# Total Genes	% D.E. Genes	UP	DOWN
E2 Ubiquitin Conjugation	33	44.42	50.00	50.00	34	23.53	50.00	50.00
E3 Ubiquitin Ligase	526	29.58	51.44	48.56	586	24.74	50.00	50.00
Deubiquitination (DUB)	72	45.83	42.00	58.00	75	24.00	41.18	58.82
Proteasome	37	36.94	59.38	40.62	37	51.35	42.86	57.14

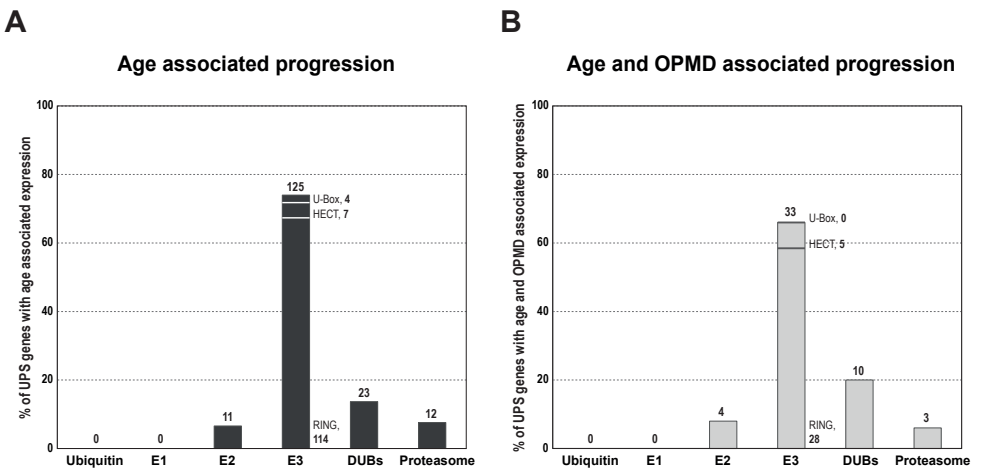

Supplementary Figure 3: Temporal changes in UPS gene expression. A linear regression was applied to identify temporal changes in expression levels of OPMD-deregulated genes in A17.1. **A)** Histogram shows the percentage of age associated OPMD-deregulated genes for each of the UPS functional components and E3-ligase subclasses. **B)** OPMD-deregulated genes showing age and OPMD associated progression. Histogram shows the percentage of genes with age and OPMD associated expression for each of the functional components. The number of genes in each bar is indicated.

Supplementary Table 5 - Deregulation of autophagy and lysosome as compared to proteasome in OPMD model systems and OPMD patients.

		Drosophila			Mouse			Human		Overlap	
	# Total Genes	% D.E. Genes	P-Value (FDR)	# Total Genes	% D.E. Genes	P-Value (FDR)	# Total Genes	% D.E. Genes	P-Value (FDR)	Mouse vs. Human # D.E. Genes	% D.E. Genes
Proteasome	47	29.79	2.15E-04	37	36.94	1.37E-07	37	51.35	9.27E-03	11	57.90
Autophagy	16	25.00	1.07E-03	39	30.77	8.13E-08	32	18.75	1.37E-02	1	16.67
Lysosome	60	5.00	1.64E-02	75	25.33	6.06E-03	73	24.66	1.54E-02	6	33.33

Additional files

Title: A list of deregulated UPS genes in mouse and human datasets.

Description: This additional file contains t-statistics (fold change and P value) for genes within the ubiquitin-proteasome pathway, in human and mouse datasets. The t-statistics represent the association of the gene expression profiles to OPMD.

Link: *http://www.skeletalmusclejournal.com/content/supplementary/2044-5040-1-15-s2.xlsx*